Radial F-actin Organization During Early Neuronal Development

Durga Praveen Meka[1§], Robin Scharrenberg[1§], Bing Zhao[1§], Theresa König[1], Irina Schaefer[1], Birgit Schwanke[1], Oliver Kobler[2], Sergei Klykov[3], Melanie Richter[1], Dennis Eggert[4], Sabine Windhorst[5], Carlos G. Dotti[6], Michael R. Kreutz[7,8], Marina Mikhaylova[3], Froylan Calderon de Anda[1*]

[1]RG Neuronal Development, Center for Molecular Neurobiology Hamburg (ZMNH), University Medical Center Hamburg-Eppendorf, 20251 Hamburg, Germany.
[2]Combinatorial Neuroimaging Core Facility (CNI), Leibniz Institute for Neurobiology, 39118 Magdeburg, Germany.
[3]Emmy-Noether Group "Neuronal Protein Transport", Center for Molecular Neurobiology (ZMNH), University Medical Center Hamburg-Eppendorf, 20251 Hamburg, Germany.
[4]Max Planck Institute for the Structure and Dynamics of Matter, 22761 Hamburg and Heinrich Pette Institute - Leibniz Institute for Experimental Virology, 20251 Hamburg, Germany
[5]Department of Biochemistry and Signal Transduction, University Medical Center Hamburg-Eppendorf, 20246 Hamburg, Germany.
[6]Centro de Biología Molecular "Severo Ochoa", CSIC-UAM, Madrid, Spain.
[7]RG Neuroplasticity, Leibniz Institute for Neurobiology, 39118 Magdeburg, Germany.
[8]Leibniz Guest Group "Dendritic Organelles and Synaptic Function", Center for Molecular Neurobiology (ZMNH), University Medical Center Hamburg-Eppendorf, 20251 Hamburg, Germany.

[§] Equal contribution

To whom correspondence should be addressed:

Froylan Calderon de Anda
Email: froylan.calderon@zmnh.uni-hamburg.de
(Tel.): +49 40 7410-56817
(Fax): +49 40 7410-56450

Abstract.

The centrosome is thought to be the major neuronal microtubule-organizing center (MTOC) in early neuronal development, producing microtubules with a radial organization. In addition, albeit in vitro, recent work showed that isolated centrosomes could serve as an actin-organizing center [1], raising the possibility that neuronal development may in addition require a centrosome-based actin radial organization. Here we report, using super-resolution microscopy and live-cell imaging, F-actin organization around the centrosome with dynamic F-actin aster-like structures with filaments extending and retracting actively. Photoconversion experiments and molecular manipulations of F-actin stability reveal a robust flux of somatic F-actin towards the cell periphery. Finally, we show that somatic F-actin intermingles with centrosomal PCM-1 satellites. Knockdown of PCM-1 and disruption of centrosomal activity not only affect F-actin dynamics near the centrosome, but also in distal growth cones. Collectively the data show a radial F-actin organization during early neuronal development, which might be a cellular mechanism for providing peripheral regions with a fast and continuous source of actin polymers; hence sustaining initial neuronal development.

The centrosome is thought to be the major neuronal microtubule-organizing center (MTOC) in early developing neurons [2-4], producing microtubules with a radial organization [5,6]. Recently, it has been shown that isolated centrosomes can serve as an actin-organizing center *in vitro* [1], suggesting that the centrosome might control F-actin organization and dynamics during initial neuronal development. However, initial attempts to demonstrate that somatic F-actin can be delivered rapidly to distal growth cones were not successful [7,8]. Moreover, the classical view on the role of actin on neuronal development is contrary to this idea. For instance, numerous studies have demonstrated that F-actin is assembled locally in growth cones and that impaired local assembly is sufficient to block neurite growth [9-13]. Nevertheless, several other studies have reported that growth cone-like structures, comprised of F-actin, have an anterograde wave-like propagation along neurites, supporting neurite extension [14-17] thus adding weight to the possibility that centrifugal actin forces starting in the cell body may contribute to the final neuronal phenotype during development. To test this possibility, we performed a series of state-of-the-art methodologies to examine actin organization and dynamics in living neurons.

We studied the micro and nano-structural organization of cytosolic F-actin near the centrosome via confocal and super-resolution microscopy during early neuronal differentiation *in vitro* (from stage 1 to early stage 3; [18]) and *in situ*. To this end the F-actin cytoskeleton in fixed and live cells was visualized via confocal and STED microscopy by labeling cells with Phalloidin-488 and Phalloidin Atto647N or SiR-actin probe [19], respectively. Confocal microscopy showed a preferential localization of cytosolic F-actin puncta near the centrosome in cultured neurons and in neurons in the developing cortex (Figure 1a-c and Supp. Figure 1a). STED microscopy images revealed that somatic F-actin organized as tightly packed structures constituted by a core of dense F-actin attached to individual F-actin filaments (aster-like structures, Figure 1d). Moreover, we used single molecule localization microscopy (SMLM / STORM) of Phalloidin-Alexa647 labeled filaments and corroborated that F-actin

organized around the centrosome in a pocket-like structure, where several F-actin puncta surrounded the centrosome with individual puncta exhibiting an aster-like organization (Supp. Figure 1b).

In order to determine whether the F-actin puncta near the centrosome represent true sites of actin polymerization, we transfected cells with Lifeact-GFP and performed epifluorescence time-lapse imaging (frame rate 2 sec for 5 min) on DIV1 neurons. The time-lapse recordings showed that the F-actin puncta in the soma are highly dynamic and intermittent. These puncta exhibit a repetitive appearance and disappearance at the same location as shown via kymographs (Supp. Figure 2a, b). Based on the duration of appearance, we categorized them as unstable (<15 sec), intermediately stable (16-240 sec), and long-lasting (241-300 sec) F-actin puncta. Quantifications show that the majority of puncta are unstable - disappearing within 15 seconds (Supp. Figure 2c), suggesting that these puncta are places of high F-actin turnover. We found that these F-actin puncta in the cell body release F-actin comets (pointed by red arrow heads in Supp. Figure 2b); thus, suggesting that they might function as a source of somatic F-actin. To gain further insight into the relevance of this conspicuous F-actin organization, we employed STED time-lapse microscopy labeling F-actin with SiR-actin (250 nM). Our analysis showed that the aster-like F-actin structures are highly dynamic, extending and retracting F-actin filaments constantly in the range of seconds (Figure 1e; Video 1). Accordingly, FRAP analysis of somatic F-actin puncta showed fast fluorescence recovery after bleaching (Supp. Figure 3a, b).

To further verify the preferential F-actin polymerization near the centrosome, we applied jasplakinolide, an agent stabilizing polymerized actin filaments and stimulating actin filament nucleation, to hippocampal primary neurons. Increasing overall F-actin nucleation should expose regions with a higher rate of actin polymerization due to an eventual depletion of monomeric actin [20]. We found that increased actin polymerization induced the formation of an F-actin ring-structure

(Supp. Figure 3c; 91.01% of 189 cells from at least three different cultures), where the highest density of plus-end microtubules labeled with EB3-mCherry can be found together with the centrosome in early developing neurons (Supp. Figure 3d). Altogether, these results unveil the existence of a complex somatic F-actin organization as well as dynamics near the centrosome, suggesting a possible role in neuronal development.

We therefore asked whether somatic actin polymerization could serve as a source for cell peripheral F-actin. To this end, we used DIV 1 neurons transfected with Lifeact-mEos3.2, which undergoes an irreversible photoconversion in response to 405 nm light from green to red fluorescence with emission peaks at 516 nm to 581 nm respectively. Interestingly, when we photoconverted a group of F-actin puncta in the soma, the intensity of the converted F-actin puncta in the soma decreased with time concomitant with a fast increase of converted signal in the cell periphery/growth cones (Figure 2a-d; Supp. Figure 4b; Video 2). Of note, we had to irradiate several F-actin puncta (5.2 to 7.1 μm^2) at once given that single punctum irradiation (2.2 μm^2) did not yield enough converted signal to trace when spreading further (Supp. Figure 4a). Another actin probe, which label F-actin and actin monomers (actin-mEos4b), also distributed into growth cones after irradiation (Figure 2c, d; Supp. Figure 4c; Video 3). However, irradiated mEos3.2 alone resulted in reduced movement of the probe and enrichment in growth cones compared to Lifeact-mEos3.2 (Figure 2c, d; Supp. Figure 4d; Video 3). To further confirm radial translocation of actin, we recorded Lifeact-mEos3.2 dynamics after pharmacological manipulation of F-actin dynamics via cytochalasin D and jasplakinolide. Supp. Figure 5 and Video 4 show that these treatments disrupted the radial translocation of the converted signal towards the cell periphery, indicating that the translocation of photoconverted signal is not due to the movement of the Lifeact probe itself but labeled F-actin.

Further characterization of photoconverted Lifeact-mEos3.2 (red signal) translocation towards the cell periphery showed that translocation does not occur

preferentially to the growth cone of the longest neurite (green asterisk in Figure 2a, e), but to the growth cone containing more F-actin (green arrow in Figure 2a and quantification in Figure 2f). In order to test whether F-actin translocation is exclusively radially-oriented, we irradiated growth cones labelled with Lifeact-mEos3.2, Actin-mEos4b, or mEos3.2. When mEos3.2 or Actin-mEos4b transfected neurons were irradiated in growth cones, the converted signal translocated towards the cell body (Figure 2h, i; Supp. Figure 6b, c; Video 5). In contrast, we found F-actin translocation to be unidirectional given that irradiation of growth cones labeled with Lifeact-mEos3.2 did not induce retrograde movement to the cell body of photoconverted Lifeact-mEos3.2 signal (Figure 2g-l, Supp. Figure 6a; Video 5).

To further confirm the F-actin translocation towards the cell periphery, we transfected neurons with Drebrin or Cofilin constructs, as F-actin stabilizing tools. Drebrin inhibits Cofilin-induced severing of F-actin and stabilizes F-actin [21,22]; Drebrin phosphorylation at S142 promotes F-actin bundling [23]. Therefore, the Drebrin phosphomimetic mutant (S142D) is a suitable candidate to decrease overall F-actin dynamics. Similarly, phosphomimetic Cofilin (S3E) is not able to severe F-actin, thus promoting F-actin stabilization [24]. In further support of our previous results, time-lapse microscopy analysis of Drebrin transfected cells revealed Drebrin to co-localize with F-actin puncta in the cell body (Supp. Figure 7a; Video 6). Moreover, transfection with the phospho-mimetic mutant Drebrin-S142D reduced F-actin treadmilling compared to cells expressing only Lifeact-GFP (Supp. Figure 7b, c). Importantly, the total number of somatic F-actin puncta decreased after Drebrin-S142D expression (Supp. Figure 7d). However, the relative amount of long lasting F-actin puncta increased (Supp. Figure 7e) and released noticeable F-actin comet-like structures towards the cell cortex (Supp. Figure 7f, Video 6).

Likewise, expression of Cofilin-S3E decreased total number of somatic F-actin puncta with an increment of long lasting F-actin puncta, compared to cells expressing only Lifeact-RFP, and reduced the F-actin treadmilling in growth cones (Supp. Figure

7b-e). Furthermore, somatic F-actin puncta acquired an aster-like appearance releasing F-actin towards the cell cortex (Supp. Figure 7g). Additionally, somatic F-actin fibers formed projections towards the cell periphery occurred (Supp. Figure 7h). Interestingly, F-actin travels along those F-actin fibers to reach the cell periphery concomitant with lamellipodia formation (Supp. Figure 7h; Video 7). Altogether, these results suggest a fast and constant delivery of F-actin towards growth cones from the somatic F-actin source.

Given that somatic F-actin puncta concentrate near the centrosome (Figure 1b), we asked whether centrosomal integrity is required for F-actin dynamics in developing neurons. We took advantage of chromophore-assisted laser inactivation (CALI) based on the genetically encoded photosensitizer KillerRed, which upon green light illumination (520-553 nm), will specifically inactivate the target protein via the generation of light-activated reactive oxygen species [25]. We fused Centrin2, a protein confined to the distal lumen of centrioles and present in the pericentriolar material, to KillerRed (Centrin2-KR) to specifically inactivate the centrosome with laser irradiation (561 nm). Cells were co-transfected with Centrin2-KR and EB3-GFP or Lifeact-GFP before plating. 24 hrs later, cells were imaged for 5 minutes (2 sec interval). Afterwards cells were exposed to the laser of 561nm for 1.5 sec. Two to three hours after laser irradiation, cells were subjected to another imaging session of 5 minutes (2 sec interval). Centrosome inactivation with CALI led to a reduced number of microtubules (Supp. Figure 8a, b; Video 8). Most importantly, we found a significant reduction of the F-actin treadmilling speed as well as the F-actin intensity at the cell periphery (Figure 3a, b; Video 9). The cells irradiated outside the centrosomal area did not show any reduction in F-actin treadmilling speed and F-actin intensity (Supp. Figure 8c, d; Video 10).

Microtubule organization in early developing neurons is centrosome-dependent [2-4]. Therefore, we decided to disrupt microtubules and to analyze whether this affects the F-actin translocation towards the cell periphery. We found that

microtubule disruption using nocodazole drastically reduced the motility of somatic photoconverted Lifeact-mEos3.2 towards the cell periphery (Figure 3c, d; Video 11). Accordingly, microtubules disruption in developing neurons leads to a less dynamic F-actin cytoskeleton [26]. Altogether, these results show that integrity of centrosome and microtubules are necessary for somatic F-actin translocation towards the cell periphery.

Next, we asked about the molecular determinants of F-actin dynamics near the centrosome. PCM-1 has been shown to promote F-actin polymerization [1] and PCM-1-containing pericentriolar satellites are important for the recruitment of proteins that regulate centrosome function [27]. The depletion of PCM-1 disrupts the radial organization of microtubules without affecting microtubule nucleation [27]. In neurons PCM-1 particles preferentially localize near the centrosome [28]. We found that PCM-1 particles intermingled with F-actin puncta in the cell soma and concentrated in proximity of F-actin puncta (Average proximity between F-actin puncta-PCM-1 = 0.584 ± 0.019 μm; Figure 4a, b). Accordingly, neurons transfected with PCM-1-GFP before plating and imaged (5 min) 24 hrs after plating, showed PCM-1-GFP granules surrounding and "touching" somatic F-actin puncta (Supp. Figure 9a; Video 12).

To further test whether PCM-1 and somatic F-actin organization are interrelated, we treated neurons (24 hrs after plating) with cytochalasin D and jasplakinolide, which interfere with actin polymerization. It has been shown for cytochalasin D treatment to induce F-actin clusters around the centrosome in non-neuronal cells [1]. Similarly, we found polarized F-actin structures, induced by cytochalasin D or jasplakinolide, which are accompanied by PCM-1 particles (Supp. Figure 9b, c). Interestingly, when cells were treated with cytochalasin D together with nocodazole, a disperse distribution of F-actin clusters (96.97%, 66 cells from at least three different cultures) associated with PCM-1 particles were formed (Supp. Figure 9d). These data indicate that actin polymerization in the cell body is linked to PCM-1 and microtubule organization.

To probe the involvement of PCM-1 more specifically we took advantage of *in utero* electroporation to introduce a PCM-1 shRNA construct that specifically silences PCM-1 expression in cortical neurons and neuronal progenitors ([28,29]; Supp. Figure 10a, c). In previous work we found PCM-1 down-regulation in the developing cortex to disrupt neuronal polarization and to preclude axon formation[28]. Furthermore, neuronal migration was impaired with piling up of neurons in the intermediate zone [28]. Here we tested the role of PCM-1 in F-actin dynamics and neurite outgrowth of cultured developing neurons and neurons differentiating in the developing cortex. We introduced PCM-1 shRNA or control shRNA plasmids together with Lifeact-GFP or Venus expressing plasmids into brain cortices at embryonic day 15 (E15), and isolated cortical neurons at E17. Neurons were cultured *in vitro* for an additional 24 hrs and were prepared for time-lapse experiments or pharmacological treatment. PCM-1 down-regulation in cultured neurons led to the formation of long and thin neurites, similar to the well-known effect induced by pharmacological F-actin disruption using cytochalasin D ([28,30]; Figure 4c; Supp. Figure 10c, d, e and f). This suggests that PCM-1 down-regulation impaired F-actin dynamics and thus boosted neurite outgrowth.

In extension of these findings, we observed a direct effect of PCM-1 down-regulation on F-actin dynamics with a reduced total number of F-actin puncta in the cell body (Figure 4c, d; Supp. Figure 10a, b). Moreover, using specific actin nucleator inhibitors (SMIFH2 and CK666), we were able to show that the somatic F-actin puncta are Formin- but not Arp2/3- dependent (Supp. Figure 11), as shown for axonal F-actin organization of mature neurons[31]. Furthermore, PCM-1 down-regulation significantly decreased the F-actin treadmilling speed (Figure 4c, e) as well as the relative F-actin levels in neurite tips (Figure 4c, f). Of note, the effects of PCM-1 knockdown were reversed when an RNAi resistant plasmid, Chicken-PCM-1-GFP, was transfected along with Lifeact-RFP and PCM-1-shRNA (Supp. Figure 12).

Finally, we tested whether PCM-1 down-regulation or F-actin disruption affect similarly neuronal differentiation in the developing cortex. We electroporated *in utero*

control shRNA or PCM-1 shRNA, together with Venus and DeAct plasmid, which impair F-actin dynamics [32], at E15 to analyze neuronal morphology at E18 *in situ*. Importantly, we found that in the developing cortex PCM-1 down-regulation and F-actin disruption in newly born neurons promote neurite elongation in a similar manner (Figure 4g-i). Thus, suggesting that PCM-1 down-regulation affects the amount of somatic F-actin, which is produced to modulate neurite outgrowth. Altogether our results show that PCM-1 regulates somatic F-actin dynamics and that somatic actin polymerization has an effect on growth cone dynamics.

Collectively, our results indicate that i) actin polymerization in the cell body preferentially occurs near the centrosome, ii) this polymerization depends on PCM-1 and microtubule integrity, and iii) somatic F-actin is released towards the cell periphery, thus affecting growth cone behavior. To our knowledge, the neuronal F-actin organization described here is a novel cellular mechanism to sustain neuronal development. Although our data do not clarify the mechanism by which somatic F-actin is delivered towards the cell periphery, our results suggest that microtubule organization is relevant for somatic F-actin delivery to growth cones. In summary, we believe our data will pave the way to future important contributions oriented to understand F-actin organization and dynamics in developing neurons.

References

1 Farina, F. *et al.* The centrosome is an actin-organizing centre. *Nat Cell Biol* **18**, 65-75, doi:10.1038/ncb3285 (2016).

2 Yau, K. W. *et al.* Microtubule minus-end binding protein CAMSAP2 controls axon specification and dendrite development. *Neuron* **82**, 1058-1073, doi:10.1016/j.neuron.2014.04.019 (2014).

3 Calderon de Anda, F., Gartner, A., Tsai, L. H. & Dotti, C. G. Pyramidal neuron polarity axis is defined at the bipolar stage. *J Cell Sci* **121**, 178-185, doi:121/2/178 [pii]10.1242/jcs.023143 (2008).

4 Stiess, M. *et al.* Axon extension occurs independently of centrosomal microtubule nucleation. *Science* **327**, 704-707, doi:science.1182179 [pii]10.1126/science.1182179 (2010).

5 Yau, K. W. *et al.* Dendrites In Vitro and In Vivo Contain Microtubules of Opposite Polarity and Axon Formation Correlates with Uniform Plus-End-Out Microtubule Orientation. *J Neurosci* **36**, 1071-1085, doi:10.1523/JNEUROSCI.2430-15.2016 (2016).

6 Sakakibara, A. *et al.* Dynamics of centrosome translocation and microtubule organization in neocortical neurons during distinct modes of polarization. *Cerebral cortex* **24**, 1301-1310, doi:10.1093/cercor/bhs411 (2014).
7 Bernstein, B. W. & Bamburg, J. R. Actin in emerging neurites is recruited from a monomer pool. *Mol Neurobiol* **6**, 95-106, doi:10.1007/BF02780546 (1992).
8 Sanders, M. C. & Wang, Y. L. Assembly of actin-containing cortex occurs at distal regions of growing neurites in PC12 cells. *J Cell Sci* **100 (Pt 4)**, 771-780 (1991).
9 Forscher, P., Lin, C. H. & Thompson, C. Novel form of growth cone motility involving site-directed actin filament assembly. *Nature* **357**, 515-518, doi:10.1038/357515a0 (1992).
10 Gallo, G., Yee, H. F., Jr. & Letourneau, P. C. Actin turnover is required to prevent axon retraction driven by endogenous actomyosin contractility. *J Cell Biol* **158**, 1219-1228 (2002).
11 Flynn, K. C. *et al.* ADF/cofilin-mediated actin retrograde flow directs neurite formation in the developing brain. *Neuron* **76**, 1091-1107, doi:10.1016/j.neuron.2012.09.038 (2012).
12 Lowery, L. A. & Van Vactor, D. The trip of the tip: understanding the growth cone machinery. *Nat Rev Mol Cell Biol* **10**, 332-343, doi:10.1038/nrm2679 (2009).
13 Okabe, S. & Hirokawa, N. Actin dynamics in growth cones. *J Neurosci* **11**, 1918-1929 (1991).
14 Ruthel, G. & Banker, G. Role of moving growth cone-like "wave" structures in the outgrowth of cultured hippocampal axons and dendrites. *Journal of neurobiology* **39**, 97-106 (1999).
15 Ruthel, G. & Banker, G. Actin-dependent anterograde movement of growth-cone-like structures along growing hippocampal axons: a novel form of axonal transport? *Cell Motil Cytoskeleton* **40**, 160-173, doi:10.1002/(SICI)1097-0169(1998)40:2<160::AID-CM5>3.0.CO;2-J (1998).
16 Flynn, K. C., Pak, C. W., Shaw, A. E., Bradke, F. & Bamburg, J. R. Growth cone-like waves transport actin and promote axonogenesis and neurite branching. *Developmental neurobiology* **69**, 761-779, doi:10.1002/dneu.20734 (2009).
17 Winans, A. M., Collins, S. R. & Meyer, T. Waves of actin and microtubule polymerization drive microtubule-based transport and neurite growth before single axon formation. *Elife* **5**, e12387, doi:10.7554/eLife.12387 (2016).
18 Dotti, C. G., Sullivan, C. A. & Banker, G. A. The establishment of polarity by hippocampal neurons in culture. *J Neurosci* **8**, 1454-1468 (1988).
19 Lukinavicius, G. *et al.* Fluorogenic probes for live-cell imaging of the cytoskeleton. *Nat Methods* **11**, 731-733, doi:10.1038/nmeth.2972 (2014).
20 Bubb, M. R., Spector, I., Beyer, B. B. & Fosen, K. M. Effects of jasplakinolide on the kinetics of actin polymerization. An explanation for certain in vivo observations. *J Biol Chem* **275**, 5163-5170 (2000).
21 Grintsevich, E. E. & Reisler, E. Drebrin inhibits cofilin-induced severing of F-actin. *Cytoskeleton (Hoboken)* **71**, 472-483, doi:10.1002/cm.21184 (2014).
22 Mikati, M. A., Grintsevich, E. E. & Reisler, E. Drebrin-induced stabilization of actin filaments. *J Biol Chem* **288**, 19926-19938, doi:10.1074/jbc.M113.472647 (2013).
23 Worth, D. C., Daly, C. N., Geraldo, S., Oozeer, F. & Gordon-Weeks, P. R. Drebrin contains a cryptic F-actin-bundling activity regulated by Cdk5 phosphorylation. *J Cell Biol* **202**, 793-806, doi:10.1083/jcb.201303005 (2013).
24 Chai, X., Forster, E., Zhao, S., Bock, H. H. & Frotscher, M. Reelin stabilizes the actin cytoskeleton of neuronal processes by inducing n-cofilin phosphorylation at serine3. *J Neurosci* **29**, 288-299, doi:10.1523/JNEUROSCI.2934-08.2009 (2009).
25 Bulina, M. E. *et al.* A genetically encoded photosensitizer. *Nat Biotechnol* **24**, 95-99, doi:nbt1175 [pii]10.1038/nbt1175 (2006).
26 Zhao, B. *et al.* Microtubules Modulate F-actin Dynamics during Neuronal Polarization. *Sci Rep* **7**, 9583, doi:10.1038/s41598-017-09832-8 (2017).

27 Dammermann, A. & Merdes, A. Assembly of centrosomal proteins and microtubule organization depends on PCM-1. *J Cell Biol* **159**, 255-266, doi:10.1083/jcb.200204023jcb.200204023 [pii] (2002).
28 de Anda, F. C., Meletis, K., Ge, X., Rei, D. & Tsai, L. H. Centrosome motility is essential for initial axon formation in the neocortex. *J Neurosci* **30**, 10391-10406, doi:30/31/10391 [pii]10.1523/JNEUROSCI.0381-10.2010 (2010).
29 Ge, X., Frank, C. L., Calderon de Anda, F. & Tsai, L. H. Hook3 interacts with PCM1 to regulate pericentriolar material assembly and the timing of neurogenesis. *Neuron* **65**, 191-203, doi:10.1016/j.neuron.2010.01.011 (2010).
30 Bradke, F. & Dotti, C. G. The role of local actin instability in axon formation. *Science* **283**, 1931-1934 (1999).
31 Ganguly, A. *et al.* A dynamic formin-dependent deep F-actin network in axons. *J Cell Biol* **210**, 401-417, doi:10.1083/jcb.201506110 (2015).
32 Harterink, M. *et al.* DeActs: genetically encoded tools for perturbing the actin cytoskeleton in single cells. *Nat Methods* **14**, 479-482, doi:10.1038/nmeth.4257 (2017).

Acknowledgements

Thanks to M. Kneussel, M. Harterink (C. Hoogenraad's laboratory) and X. Chai (M. Frotscher's labaratory) for plasmid constructs. Thanks to the laboratories of M. Kneussel and P. Soba at the ZMNH for equipment use. Thanks to I. Hermans-Borgmeyer and members of UKE-Hamburg animal facility for their help with animal experiments.

M. Kreutz is supported by the Leibniz Foundation, Deutsche Forschungsgemeinschaft (Kr1879 5-1, 6-1; SFB 779 TPB8), BMBF Energi and JPND STAD. M. Mikhaylova is supported by grants from the Deutsche Forschungsgemeinschaft (DFG Emmy-Noether Programm (MI 1923/1-1) and FOR2419 (MI 1923/2-1). O. K. is funded by the DFG Grant SCHE 132/18-1. F. Calderon de Anda is supported by Deutsche Forschungsgemeinschaft (DFG) Grants (FOR 2419: CA1495/1-1; and CA 1495/4-1), ERA-NET Neuron Grant (Bundesministerium für Bildung und Forschung, BMBF, 01EW1410 ZMNH AN B1), Landesforschungsförderung Hamburg (Z-AN LF), and University Medical Center Hamburg-Eppendorf (UKE).

Additional Information

Competing financial interest: The author(s) declare no competing financial interests.

Figure 1. Super-resolution microscopy reveals cytosolic F-actin puncta releasing filaments in developing neurons. (a) Stage 2 hippocampal neuron labelled with phalloidin and Pericentrin antibody, confocal z-stacks from the inset show F-actin puncta around the centrosome. (**b**) Rose plots depict distribution of F-actin puncta (cortical and cytosolic or only cytosolic) in the cell body with respect to the position of the centrosome. The proximity of cytosolic F-actin puncta with centrosome was shown, 10% or 20% distance range from the total area is indicated in different shades of blue; n = 12 cells, obtained from at least three different cultures. (**c**) Multipolar cell located in the IZ of the developing cortex express Lifeact-GFP and Centrin2-RFP and shows F-actin puncta surrounding the centrosome in the developing cortex. (**d**) Confocal (CLSM) and STED microscopic images of stage 2 hippocampal neuron. Inset: STED Z-stack images with 160 nm Z-spacing showing F-actin puncta localizing near the centrosome. Insets from arrowheads in Z-stack images show F-actin puncta with F-actin fibers attached. (**e**) Confocal image of stage 2 neuron labeled with SiR-actin (250nM). Inset 1:snap shot of STED time-lapse. Time-lapse montages from insets 2 and 3 depict individual F-actin puncta releasing F-actin fibers (arrowheads). Time (t) interval = 1.7 sec (Video 1). Scale bar: 10 μm (a, c and d); 2 μm (e); 0.5 μm (inset e).

Figure 2. Somatic F-actin puncta act as rapid supply sources of F-actin to the periphery in developing neurons. (**a**) Representative images of stage 2 cell expressing Lifeact-mEos3.2. Cell was irradiated at red circle with 405 nm laser for converting green signal to red. Time-lapse image of the cell before (green signal) and after photoconversion (red signal) at indicated time points. Red arrowheads point reach of the photoconverted signal. Green arrowheads point to the growth cone with more Lifeact-Eos signal before and after photoconversion. (**b**) Inset of photoconversion area, before photoconversion (green). Kymographs obtained from white-line showing

photoconversion of F-actin puncta. Arrowhead shows time of 405-laser irradiation. (**c**) Comparison of normalized intensity values in the photoconverted area of cells expressing Lifeact-mEos3.2, Actin-mEos4b or mEos3.2 during the first 120 sec after photoconversion. Half-time (t ½) values are shown in the inset graph. Lifeact-mEos3.2 = 14.71 ± 1.191, mEos3.2 = 40.47 ± 3.130 and Actin-mEos4b = 13.38 ± 0.7721. $p<0.0001$ by one-way ANOVA, post hoc Dunnett's test, ***$p<0.001$. Mean ± SEM, n =18 cells for Lifeact-mEos3.2, n = 13 cells for mEos3.2 and n = 16 cells for Actin-mEos4b. (**d**) Growth cone to soma intensity ratio of photoconverted signal from cells expressing Lifeact-mEos3.2, Actin-mEos4b and mEos3.2 during first 50 sec after photoconversion. Ymax values are shown in the graph. Lifeact-mEos3.2 = 0.1900 ± 0.02575, mEos3.2 = 0.04493 ± 0.008169 and Actin-mEos4b = 0.1736 ± 0.02283. $p<0.0001$ by one-way ANOVA, post hoc Dunnett's test, ***$p<0.001$, n.s = not significant. Mean ± SEM, n = 12 cells for Lifeact-mEos3.2, n = 11 cells for mEos3.2 and n = 9 cells for Actin-mEos4b. (**e**) Normalized intensity in growth cones from cells expressing Lifeact-mEos3.2, Actin-mEos4b and mEos3.2 during first 120 sec after photoconversion. Lines indicate fitted exponential equations. Inset graph shows normalized intensity in growth cones of indicated groups on a logarithmic scale. (**f**) Pearson correlation of growth cone to soma intensity ratio before and after photoconversion. n=57 neurites from 11 Lifeact-mEos3.2 cells; Pearson r = 0.731, $p<0.0001$. (**g**) Representative images of stage 2 cell expressing Lifeact-mEos3.2 was irradiated in the growth cones with 405 nm laser (red circle) for photoconversion of the green signal to red. Images of the cell before (green) and after (red) photoconversion at indicated time points of the time-lapse were shown. Red arrowheads point the reach of the photoconverted signal over time. (**h**) Comparison of normalized intensity values in the photoconverted area (growth cones) of cells expressing Lifeact-mEos3.2, Actin-mEos4b or mEos3.2 during the first 120 sec after photoconversion. Half-time (t ½) values are shown in the inset graph. Lifeact-mEos3.2 = 30.37 ± 4.012, mEos3.2 = 18.25 ± 3.684 and Actin-mEos4b = 18.41 ± 2.143. $p=0.1385$ by one-way ANOVA, post

hoc Dunnett's test, n.s = not significant. Mean ± SEM, n = 3 cells for Lifeact-mEos3.2, n = 7 cells for mEos3.2 and n = 3 cells for Actin-mEos4b. (**i**) Normalized intensity of photoconverted signal in the soma of Lifeact-mEos3.2, Actin-mEos4b and mEos3.2 expressing cells during the first 120 sec after photoconversion. Ymax values are shown in the inset graph. Lifeact-mEos3.2 = 3.112 ± 0.9059, mEos3.2 = 33.98 ± 2.354 and Actin-mEos4b = 8.726 ± 3.864. p<0.0001 by one-way ANOVA, post hoc Dunnett's test, ****p<0.0001, n.s = not significant. Mean ± SEM, n = 3 cells for Lifeact-mEos3.2, n = 7 cells for mEos3.2 and n = 3 cells for Actin-mEos4b. Scale bar: 10 μm.

Figure 3. Centrosome inactivation affects F-actin intensity and treadmilling in growth cones. (**a**) Neurons transfected with Centrin2-KillerRed and Lifeact-GFP subjected to localized CALI treatment. Upper panel: Centrin2-KR signal before and after treatment; Middle and lower panels: Kymograph of actin treadmilling in growth cone before and after CALI treatment (**b**) Influence of CALI on F-actin treadmilling speed and F-actin intensity in growth cones. Treadmilling speed (in μm/min): before treatment= 4.598 ± 0.1596, after treatment: 2.314 ± 0.1133. ****p < 0.0001 by paired Student's t-test. Mean ± SEM; n=10 cells from at least three different cultures. F-actin intensity (%): before treatment = 100.0 ± 6.168, after treatment: 82.97 ± 5.335. ****p < 0.0001 by paired Student's t-test. Mean ± SEM; n=10 cells from at least three different cultures. (**c**) Representative images of a neuron expressing Lifeact-mEos3.2 treated with 7uM Nocodazole. Irradiation was performed at red circle with 405 nm laser for photoconversion. Images of the cell before (green) and after photoconversion (red) at indicated time points of the time-lapse. Arrowheads point no movement in the photoconverted signal. (**d**) Intensity change during the first 20 sec after photoconversion in the soma and growth cone regions of untreated and Nocodazole treated cells expressing Lifeact-mEos3.2. Somatic region: untreated = -1.541 ± 0.06428, nocodazole = -3.222 ± 1.175. Growth cone region: untreated = 0.4248 ±

0.05893, nocodazole = 0.07202 ± 0.06966, **p<0.01 by unpaired Student's t-test. Mean ± SEM; n = 12 cells for untreated and n=8 cells for nocodazole groups. Cells were obtained from at least two different cultures. Scale bar: 10 μm.

Figure 4. PCM-1 intermingles with F-actin puncta and is essential for the maintenance of F-actin in the soma and growth cones. (**a**) Confocal Max projection of stage 2 hippocampal primary neuron stained with PCM-1 antibody and phalloidin showing polarized and intermingled PCM-1, F-actin puncta. (**b**) Nearest neighbor analysis showing frequency distribution of proximity distance between actin-actin puncta (black bars), actin-PCM-1 puncta (red bars) and PCM-1–PCM-1 puncta (green bars). Average proximity values are shown in inset graph; actin-actin = 0.8280 ± 0.0178, actin-PCM-1 = 0.5840 ± 0.0193 and PCM-1–PCM-1 = 0.8057 ± 0.0345. Mean ± SEM, n = 5 cells. (**c**) Representative images of DIV I cortical neurons transfected with either control or PCM-1 shRNA together with Lifeact-GFP. Kymographs are obtained from lines marked as 1 and 3 for soma of control and PCM-1 shRNA, respectively. Lines 2 and 4 for growth cones of control and PCM-1 shRNA, respectively. (**d**-**f**) Quantifications of control (control shRNA + Lifeact-GFP) and PCM-1 shRNA (PCM-1 shRNA + Lifeact GFP) conditions: (**d**) Normalized F-actin puncta/μm^2 somatic area of stage 2 cells from control condition = 1.000 ± 0.0690, PCM-1 shRNA condition = 0.7122 ± 0.05809; **p= 0.0078 by unpaired Student's t-test. Mean ± SEM; n = 7 cells each for control and PCM-1 shRNA. Cells were obtained from at least three different cultures. (**e**) F-actin treadmilling speed (μm/min) in growth cones (or neurite tips for PCM-1 shRNA cells) of stage 2 cells from control condition = 5.2452 ± 0.2064; PCM-1 shRNA condition = 2.4402 ± 0.1543; ****p<0.0001 by unpaired Student's t-test. Mean ± SEM; n=10 cells for control and PCM-1 shRNA. Cells were obtained from at least three different cultures. (**f**) F-actin intensity ratio in growth cones of control condition = 0.9979 ± 0.0526, neurite tips of PCM-1 shRNA condition = 0.6513 ± 0.0401. ****p<0.0001 by unpaired Student's t-test. Mean ± SEM; n = 10 cells for

control, n = 8 cells for PCM-1 shRNA groups. Cells were obtained from at least two different cultures. (**g**) Cortical slices showing migrating multipolar cells in the intermediate zone (IZ) of E18 mouse brain embryos that were *in utero* electroporated at E15 with control shRNA or PCM-1 shRNA or DeAct plasmids together with Venus or mCherry. PCM-1 downregulation or actin depolymerization (via DeAct expression) resulted in neurite elongation and increase in neurite terminals of cells in the intermediate zone (IZ). (**h**) Left panel: Total length of neurites per cell in control condition = 160 ± 19.37, PCM-1 shRNA = 228.5 ± 16.82, and DeAct expressing cells = 227 ± 16.71. $p=0.0123$ by one-way ANOVA, post hoc Dunnett's test. *$p<0.05$. Mean ± SEM; n = 15 cells from three brains in each group. Right panel: Number of neurite terminals per cell in control condition = 8.133 ± 0.88, PCM-1 shRNA = 11 ± 0.66, and DeAct expressing cells = 10.87 ± 0.93. $p=0.0321$ by one-way ANOVA, post hoc Dunnett's test. *$p<0.05$. Mean ± SEM; n = 15 cells from three brains in each group. Scale bar: 10 μm.

Figure 1

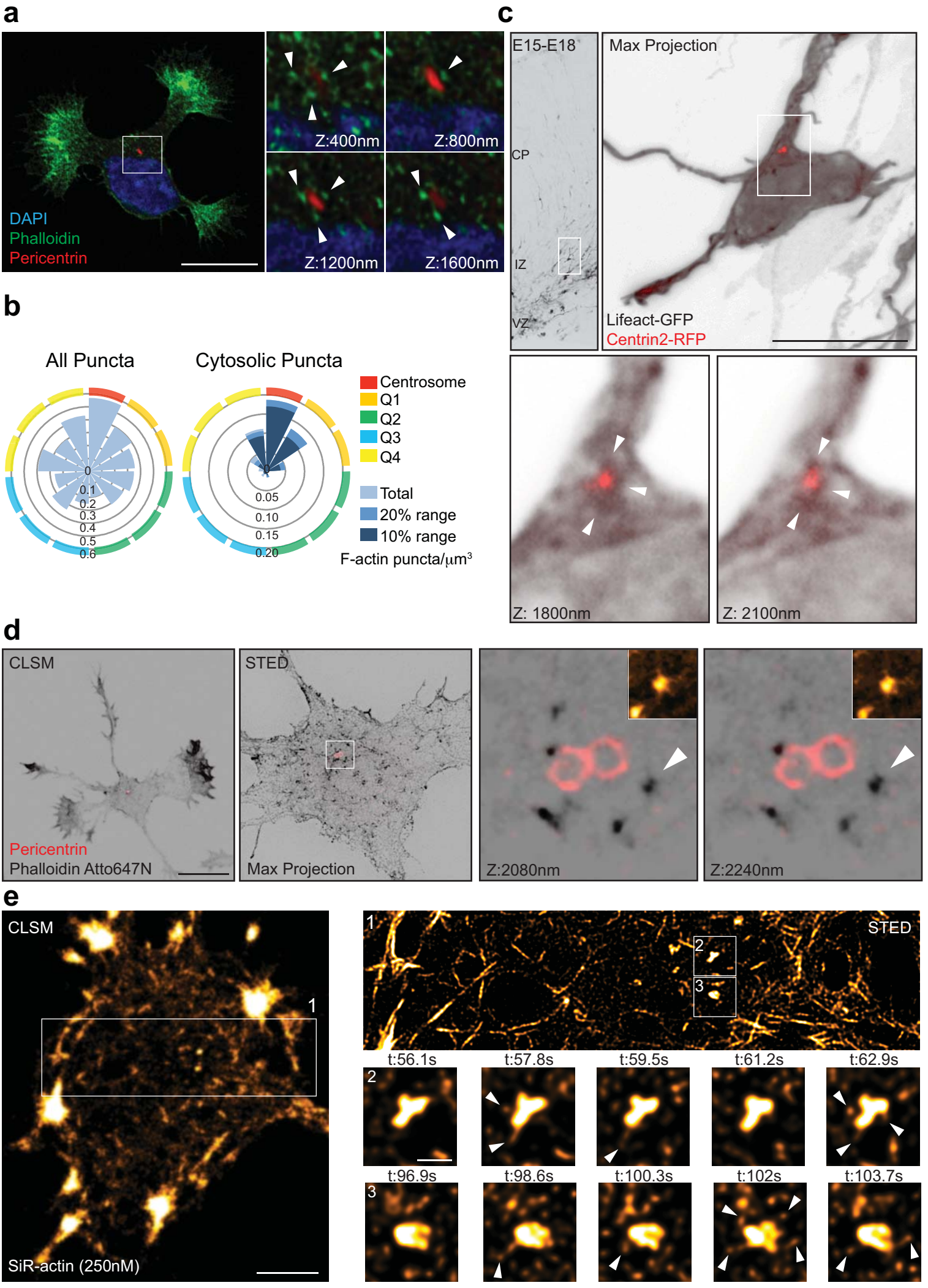
a
DAPI
Phalloidin
Pericentrin
Z:400nm
Z:800nm
Z:1200nm
Z:1600nm
b
All Puncta
Cytosolic Puncta
0
0.1
0.2
0.3
0.4
0.5
0.6
0.05
0.10
0.15
0.20
Centrosome
Q1
Q2
Q3
Q4
Total
20% range
10% range
F-actin puncta/μm³
c
E15-E18
CP
IZ
VZ
Max Projection
Lifeact-GFP
Centrin2-RFP
Z: 1800nm
Z: 2100nm
d
CLSM
Pericentrin
Phalloidin Atto647N
STED
Max Projection
Z:2080nm
Z:2240nm
e
CLSM
1
SiR-actin (250nM)
STED
2
3
t:56.1s
t:57.8s
t:59.5s
t:61.2s
t:62.9s
t:96.9s
t:98.6s
t:100.3s
t:102s
t:103.7s

Figure 2

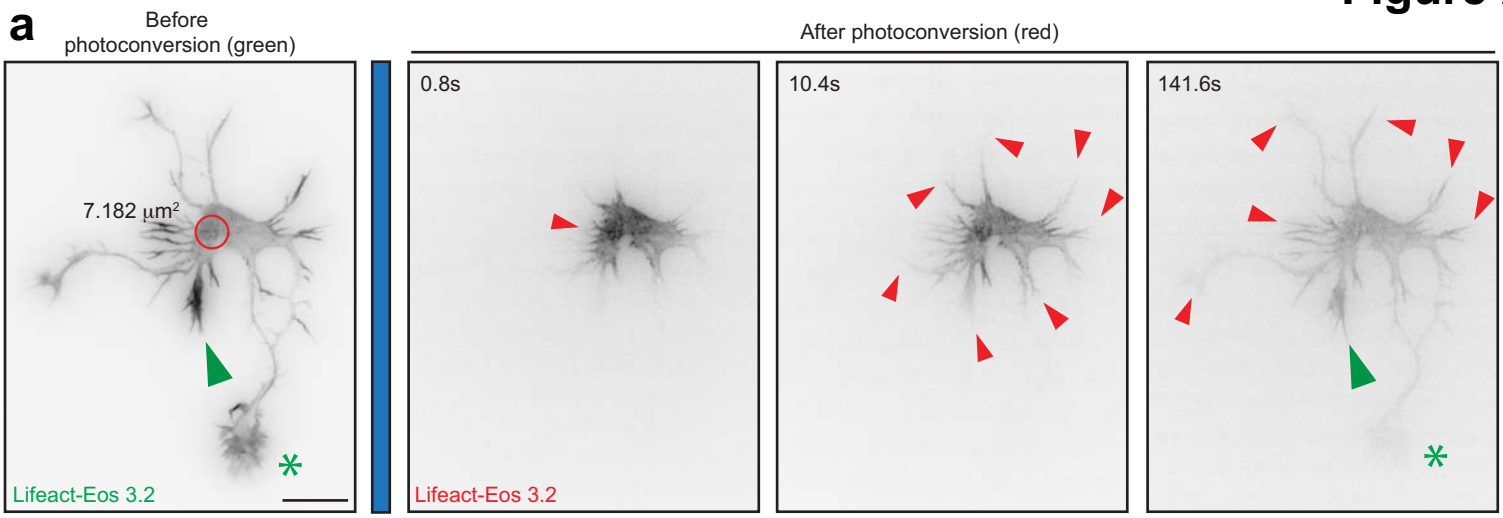
a
Before photoconversion (green)
After photoconversion (red)
7.182 μm²
0.8s
10.4s
141.6s
Lifeact-Eos 3.2
Lifeact-Eos 3.2

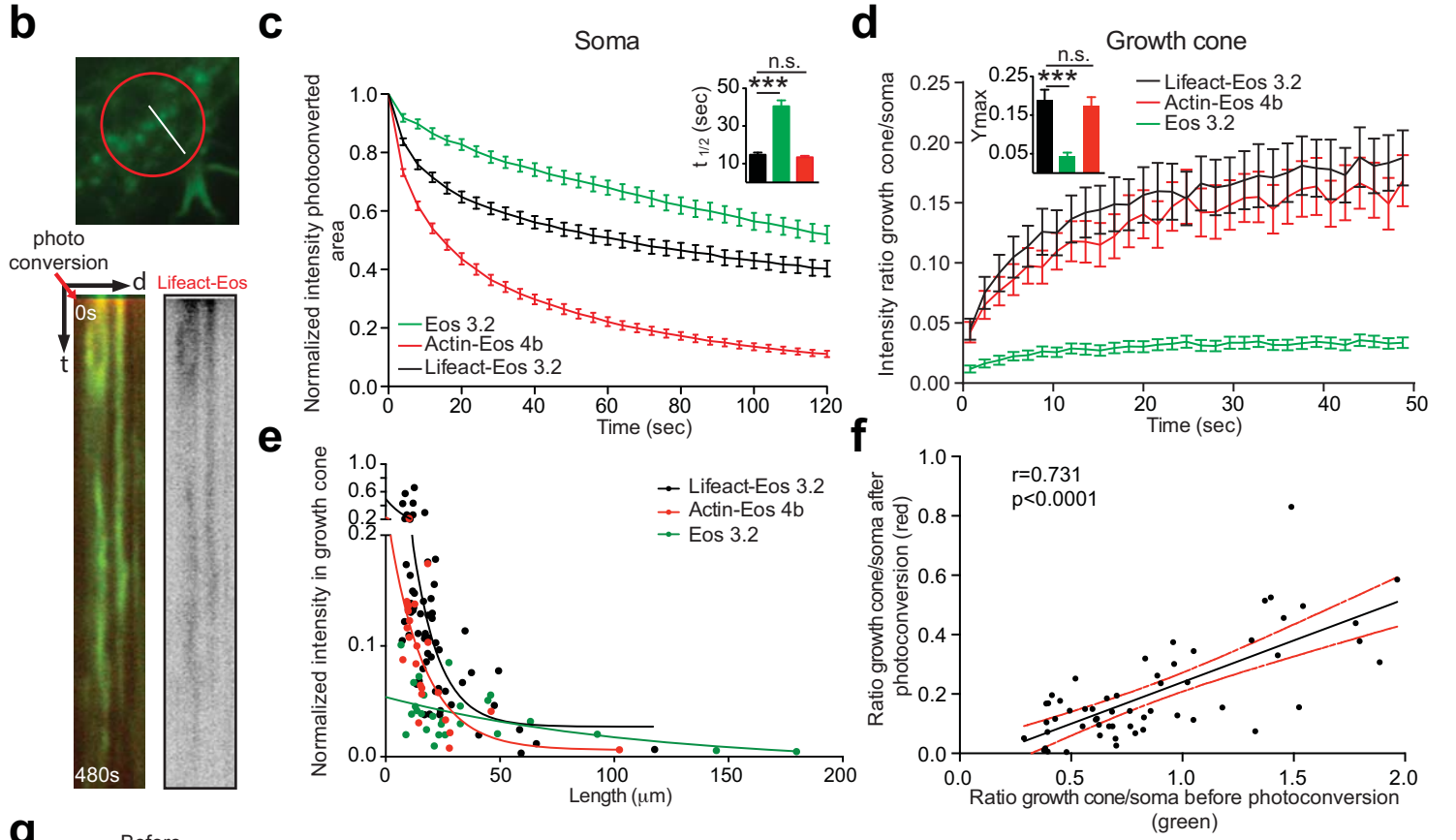
b
photo conversion
d
Lifeact-Eos
0s
t
480s
c
Soma
Normalized intensity photoconverted area
Time (sec)
Eos 3.2
Actin-Eos 4b
Lifeact-Eos 3.2
n.s.
***
t 1/2 (sec)
d
Growth cone
Intensity ratio growth cone/soma
Time (sec)
Ymax
e
Normalized intensity in growth cone
Length (μm)
f
r=0.731
p<0.0001
Ratio growth cone/soma after photoconversion (red)
Ratio growth cone/soma before photoconversion (green)

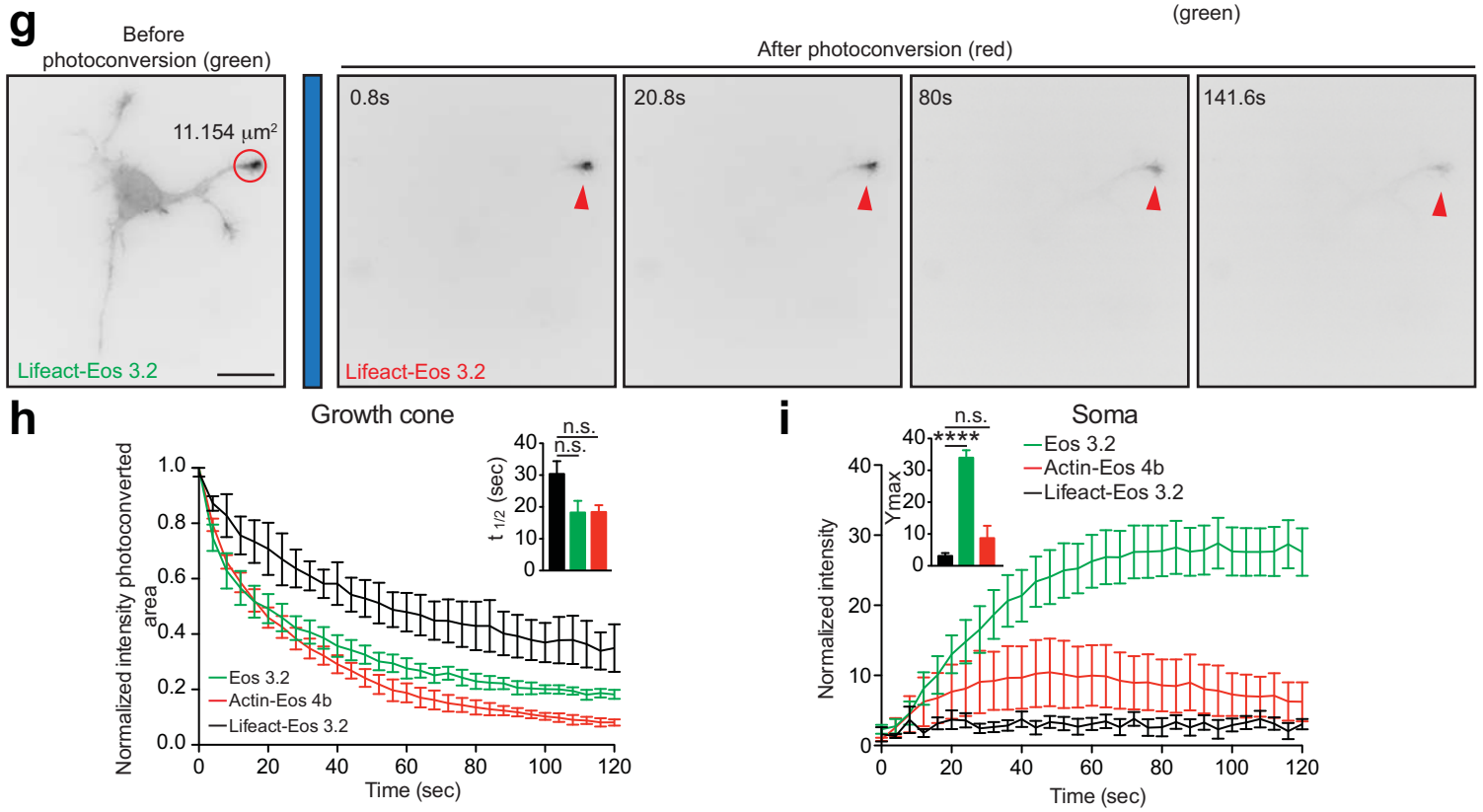
g
Before photoconversion (green)
After photoconversion (red)
11.154 μm²
0.8s
20.8s
80s
141.6s
Lifeact-Eos 3.2
Lifeact-Eos 3.2
h
Growth cone
Normalized intensity photoconverted area
Time (sec)
Eos 3.2
Actin-Eos 4b
Lifeact-Eos 3.2
n.s.
t 1/2 (sec)
i
Soma
Normalized intensity
Time (sec)
****
Ymax

Figure 3

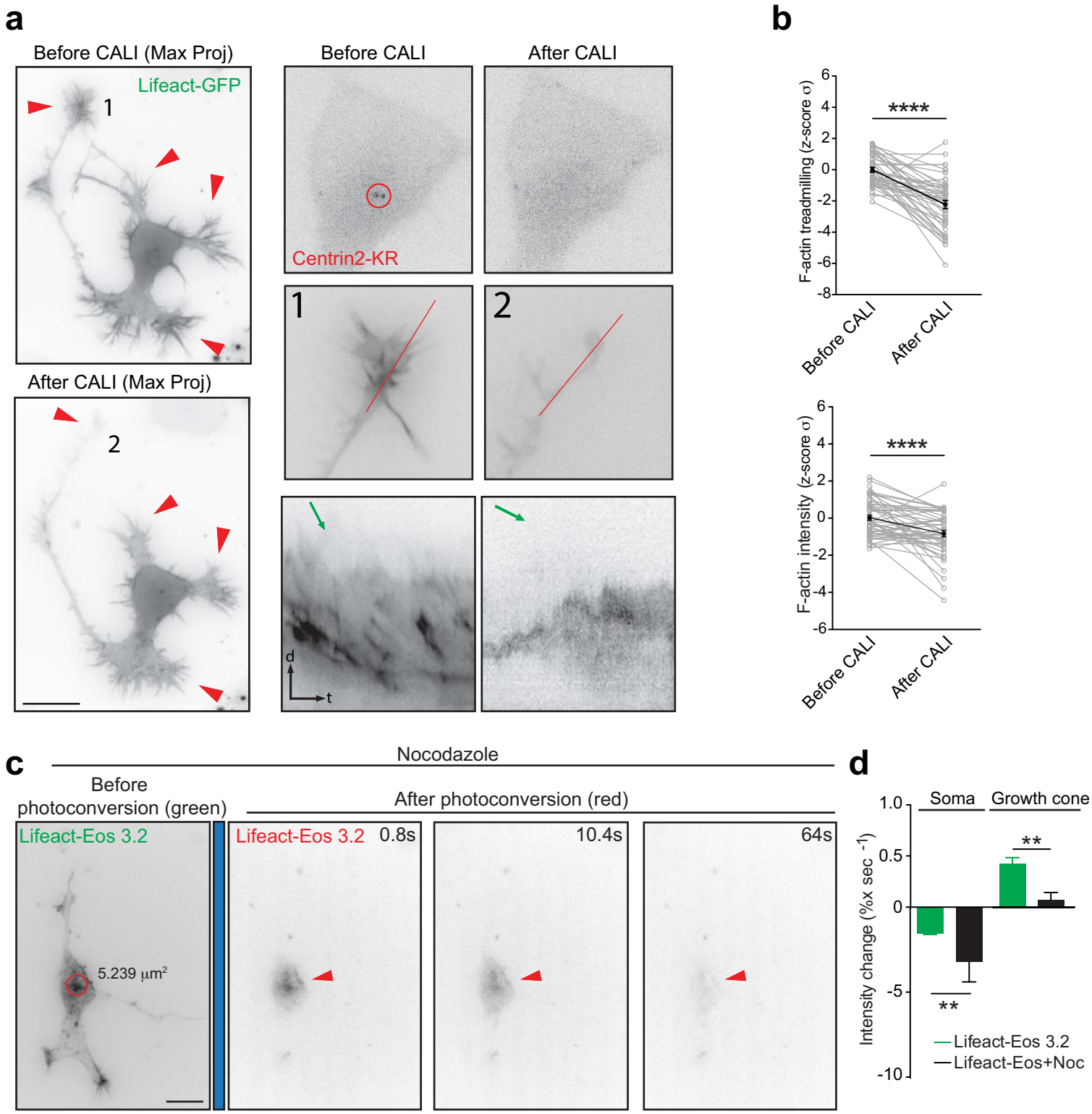
a
Before CALI (Max Proj)
Lifeact-GFP
1
After CALI (Max Proj)
2
Before CALI
After CALI
Centrin2-KR
1
2
d
t
b
F-actin treadmilling (z-score σ)
****
Before CALI
After CALI
F-actin intensity (z-score σ)
****
Before CALI
After CALI
c
Nocodazole
Before photoconversion (green)
After photoconversion (red)
Lifeact-Eos 3.2
5.239 μm²
Lifeact-Eos 3.2 0.8s
10.4s
64s
d
Soma
Growth cone
Intensity change (%x sec⁻¹)
**
**
Lifeact-Eos 3.2
Lifeact-Eos+Noc

Figure 4

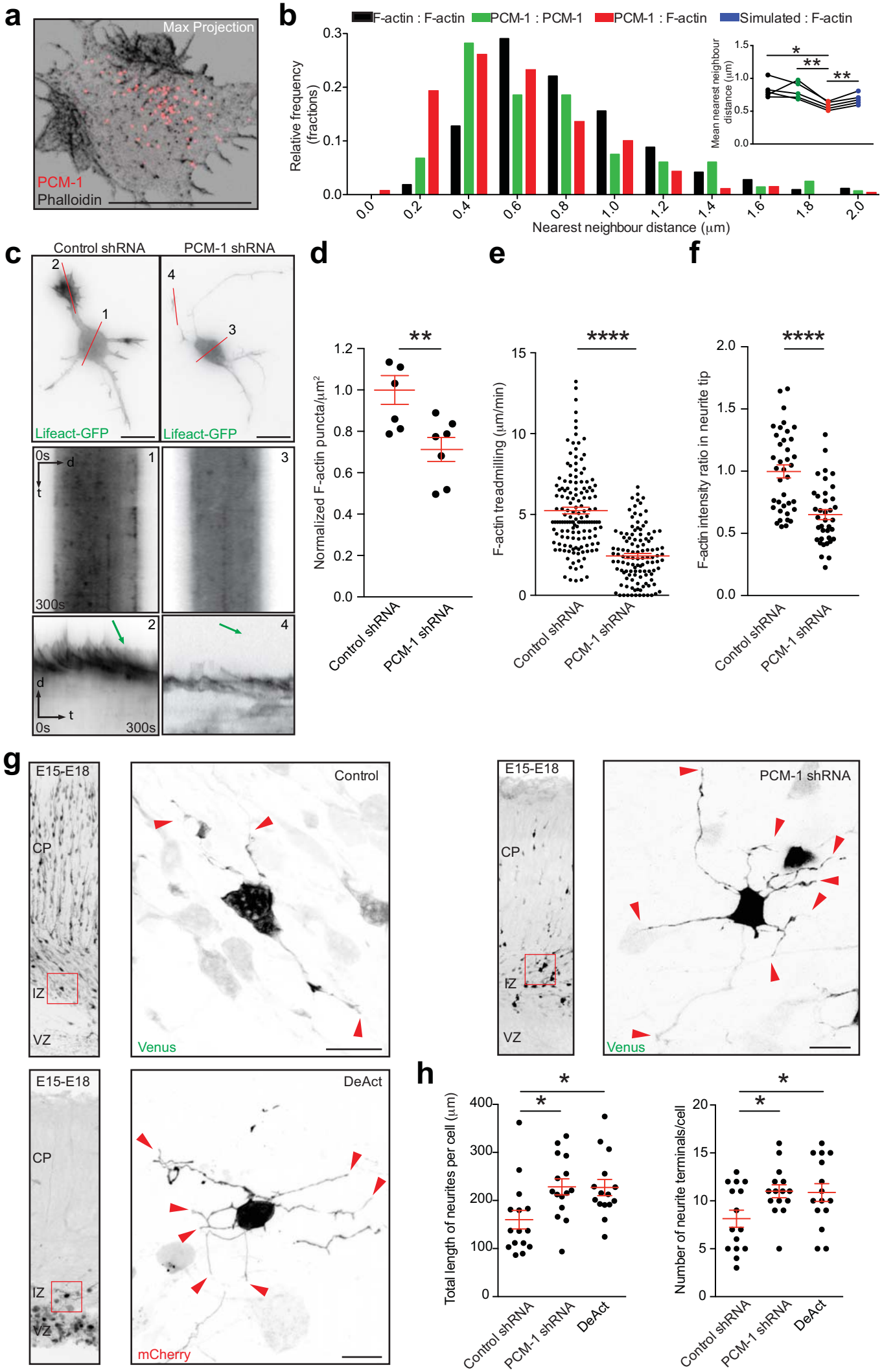
a
Max Projection
PCM-1
Phalloidin
b
F-actin : F-actin
PCM-1 : PCM-1
PCM-1 : F-actin
Simulated : F-actin
Relative frequency (fractions)
Nearest neighbour distance (μm)
Mean nearest neighbour distance (μm)
c
Control shRNA
PCM-1 shRNA
Lifeact-GFP
0s
300s
d
Normalized F-actin puncta/μm²
e
F-actin treadmilling (μm/min)
f
F-actin intensity ratio in neurite tip
g
E15-E18
CP
IZ
VZ
Control
Venus
PCM-1 shRNA
DeAct
mCherry
h
Total length of neurites per cell (μm)
Number of neurite terminals/cell